Optical Gating of Resonance Fluorescence from a Single Germanium Vacancy Color Center in Diamond

Disheng Chen,[1,2,*] Zhao Mu,[1,*] Yu Zhou,[1] Johannes E. Fröch,[3] Abdullah Rasmit,[1] Carole Diederichs,[4,5] Nikolay Zheludev,[1,2,6] Igor Aharonovich,[3,†] and Wei-bo Gao[1,2,‡]

[1]*Division of Physics and Applied Physics, School of Physical and Mathematical Sciences, Nanyang Technological University, Singapore 637371, Singapore*

[2]*The Photonics Institute and Centre for Disruptive Photonic Technologies, Nanyang Technological University, Singapore 637371, Singapore*

[3]*School of Mathematical and Physical Sciences, University of Technology Sydney, Ultimo, New South Wales 2007, Australia*

[4]*Laboratoire de Physique de l'Ecole Normale Supérieure, ENS, Université PSL, CNRS, Sorbonne Université, Université de Paris, 75005 Paris, France*

[5]*MajuLab, International Joint Research Unit UMI 3654, CNRS, Université Côte d'Azur, Sorbonne Université, NUS, NTU, Singapore 117543, Singapore*

[6]*Optoelectronics Research Centre, University of Southampton, Hampshire, SO17 1BJ, United Kingdom*

(Received 25 January 2019; published 19 July 2019)

Scalable quantum photonic networks require coherent excitation of quantum emitters. However, many solid-state systems can undergo a transition to a dark shelving state that inhibits the resonance fluorescence. Here, we demonstrate that by a controlled gating using a weak nonresonant laser, the resonant fluorescence can be recovered and amplified for single germanium vacancies. Employing the gated resonance excitation, we achieve optically stable resonance fluorescence of germanium vacancy centers. Our results are pivotal for the deployment of diamond color centers as reliable building blocks for scalable solid-state quantum networks.

DOI: 10.1103/PhysRevLett.123.033602

Artificial atomic systems that can be coherently controlled and manipulated are of paramount importance for the realization of scalable quantum photonic architectures [1,2]. Recently, color centers in diamond, particularly group IV defects, such as the silicon vacancies (SiV) [3] or the germanium vacancies (GeV) [4–9] have emerged as attractive candidates. These defects possess an inversion symmetry [10] and therefore are not sensitive to local fluctuation in electric fields, resulting in a robust optical fluorescence with high indistinguishability [11]. An additional advantage of those systems is their high Debye-Waller factor that is manifested in a significant portion of the emission being concentrated in the zero phonon line (ZPL) [5,12]. This high concentration makes their resonance fluorescence (RF) appealing for efficient long-distance quantum communication [13], quantum teleportation [14], and entanglement swapping [15].

Unfortunately, under resonant excitation, these systems can undergo a nonradiative transition to a dark state, resulting in a quenching of RF. For the nitrogen vacancy (NV) centers [16], this is often associated with a charge-state transition from negative to neutral [17,18]. Such a process results in the lack of photons under resonant excitation, and consequently hinders the potential for single-shot spin readout [19,20], and continuous operation of the quantum network [21]. Here, we show that the quenching of RF also occurs for GeV color centers. On the positive side, we find that the RF can be reinstated by employing a small amount of nonresonant beam at 532 nm without inducing any additional spectral diffusion on the quantum emitter. This laser acts as a gate control over the fluorescence from the emitter, which can be quantitatively modeled by using a two-level system accompanied by a dark state.

The investigated sample consists of implantation-generated GeV centers within an electronic-grade Type IIa diamond [22]. The implanted Ge atom takes the interstitial space between the two empty carbon sites, forming a unique split-vacancy configuration with D_{3d} symmetry, as shown in Fig. 1(a). Because of the strong spin-orbit coupling [27], the ground state (^2E_g) and excited state (^2E_u) split into a pair of energy levels with twofold spin degeneracy at zero magnetic field, leading to the characteristic four-line fine structure in the ZPL emission spectrum at 602 nm [Fig. 1(b)]. To enhance the photon collection efficiency, a half-sphere solid immersion lens (SIL) with a diameter of 5 μm is fabricated on top of the sample by using focused ion (Ga+) beam (FIB) milling before Ge implantation [22,28], as shown in Fig. 1(c). The sample is mounted on a XYZ piezostepper motorized stage housed in a closed-cycle helium-flow cryostat at 5 K. The second-order autocorrelation measurement confirms the singleness of the emitter, as shown in Fig. 1(d).

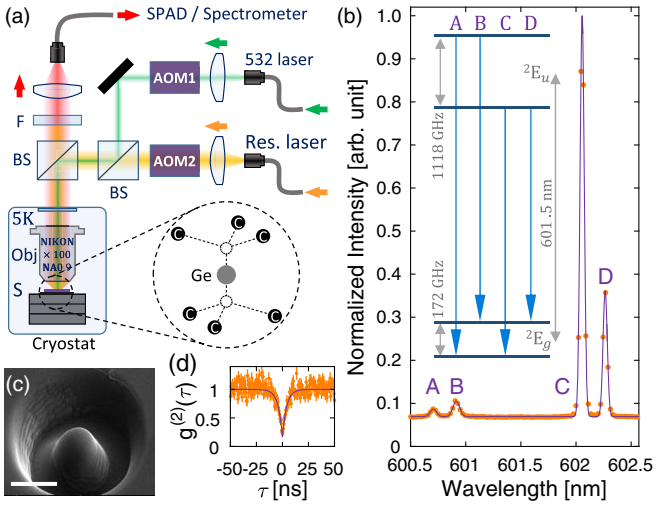

FIG. 1. (a) Experimental setup. AOM, acousto-optic modulator; BS, 50:50 nonpolarizing beam splitter; Obj, objective; S, sample; F, spectral filter; SPAD, single-photon avalanche detector. Inset, schematic of a GeV center. (b) Normalized PL spectrum of the GeV color center at 5 K, excited at 532 nm with a power of 0.4 mW ($0.06P_1$) for an exposure time of 5 s. The purple line is the fitting with four Gaussian peaks, labeled as A, B, C, and D from high to low energy. Inset, energy structure of the GeV center with four optical transitions labeled according to the spectrum. Splitting reflects the best-fit parameters. (c) Scanning electron microscope (SEM) image of a FIB milled SIL. Scale bar, 3 μm. (d) Room temperature second-order autocorrelation function $g^{(2)}(\tau)$ of the GeV center under nonresonant excitation (532 nm, $\sim$1 mW). Fitting with single exponential decay (solid line) gives $g^{(2)}(0) = 0.17 \pm 0.03$.

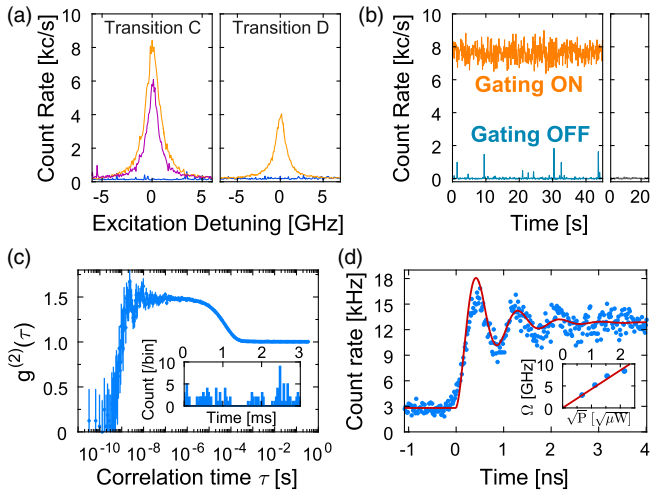

FIG. 2. (a) PLE spectra of transitions C (left) and D (right) when the gating laser at 532 nm is on (orange) and off (blue). The purple curve corresponds to the gating wavelength at 405 nm. Zero detuning corresponds to 602.2903 and 602.4828 nm for C and D, respectively. (b) RF intensity of transition C for gating on (orange) and gating off (blue). Right, PL intensity under solely nonresonant excitation. Background has been subtracted from the data. Bin size, 100 ms. (c) $g^{(2)}(\tau)$ of the GeV center under resonant pumping of transition C. $g^{(2)}(0) = 0.07$. The oscillatory signal at $\tau \approx 5$ ns is the Rabi oscillations induced by resonant pumping. Inset, stochastic jump of the RF. Bin size, 33 μs. (d) Rabi oscillations of transition C in pulsed measurement. Red curve is a fitting by the two-level system [22]. Inset, Rabi frequency against the square root of resonant power with a linear fit (red). Resonant power is 200 nW for (a) and (b), 300 nW for (c), and 2.4 μW for (d). Nonresonant power is 1.2 μW (1.8×10^{-4} P_1) for all.

All optical measurements are performed by using a homebuilt confocal microscope, as shown in Fig. 1(a). An achromatic microscopic objective with NA = 0.9 is placed one focal length away from the sample to focus the excitation beam into the SIL and collect the the photoluminescence (PL) from the emitter. A tunable continuous-wave (cw) laser with a linewidth of <1 MHz is used to resonantly address the GeV center, and perform photoluminescence excitation (PLE) measurements. A diode-pumped solid-state laser at 532 nm is used for nonresonant excitation of the emitter and gating of RF, enabled by passing through an acousto-optic modulator (AOM). After it is directed through a bandpass filter, the PL is coupled into a single-mode fiber connected to a spectrometer or a single-photon avalanche detector (SPAD). In PL spectrum characterization, a 600 ± 7 nm bandpass filter is used for ZPL detection; in PLE and gating experiments, a 650 ± 20 nm bandpass filter is used for phonon-side band PL detection.

The gating effect by the nonresonant laser can be demonstrated by comparing PLE spectra with the gating laser on or off, as shown in Fig. 2(a). For both transitions C and D, the PLE spectra are only detectable when the gating laser is on. The PL intensity is enhanced by 500-fold when switching on the gating laser, as shown in Fig. 2(b), where the gating power is $\sim 10^{-4}$ of nonresonant saturation power $P_1 = 6.8 \pm 0.1$ mW [22]. In fact, this nonresonant beam is too weak to induce any detectable fluorescence from the emitter [right panel of Fig. 2(b)], and the main role played by this light is a switch controlling the on and off of the RF from the emitter. By normalizing the PL intensity to the number of photons in the gating beam, we find that 405 nm nonresonant beam generates a nearly identical gating efficiency as of 532 nm [22], as shown in Fig. 2(a).

We stress that the optical pumping between the two ground states cannot account for these observations because the orbital relaxation, $T_1^{\text{orbital}} \simeq 20$ ns [29], is orders of magnitude faster than the gating dynamics involved here. Instead, a long-lived dark state is resorted for the explanation, evident by the bunching plateau of second-order correlation function and the stochastic jumping of RF, as shown in Fig. 2(c) [30,31]. Even with the presence of a dark state, coherence between the ground and excited states can still be generated and maintained for a coherence time of $T_2 = 366 \pm 20$ ps, as shown by the Rabi oscillations of transition C in Fig. 2(d). Since we do observe multiple peaks around transition C for some measurements [see Fig. S5(a) in Supplemental Material [22]], we focus on transition D for the rest of the Letter for the sake of clarity.

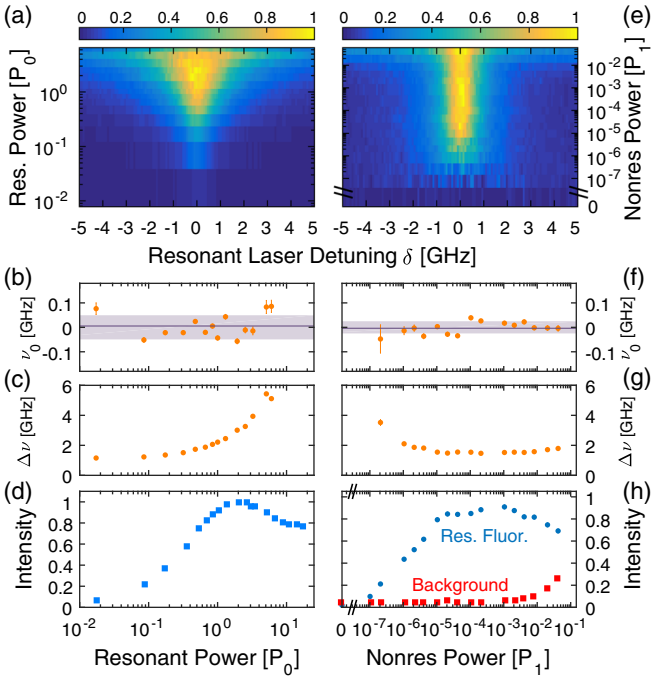

FIG. 3. 2D map of normalized PLE spectra (transition D) by varying (a) the resonant excitation power, or (e) the nonresonant excitation power. Normalization constant, (a) 10 kcnt/s and (e) 4 kcnt/s. Gating power in (a), $7 \times 10^{-5} P_1$; resonant power in (e), $0.35 P_0$. (b) and (f) are the center frequency ν_0 of each line in (a) and (e), respectively, extracted from Lorentzian fitting. The shaded region represents the standard deviation of ν_0, (b) $\sigma \sim 50$ MHz, and (f) $\sigma \sim 25$ MHz. (c) and (g) are the Lorentzian linewidth $\Delta\nu$ of each line in (a) and (e), respectively. (d) Resonant-power dependence of RF, measured by setting the resonant laser at zero detuning. (h) Gating-power dependence of RF (blue), evaluated by subtracting the background from the maximum count rate of each line in (e). Background count rate (red) is measured at a far detuning of ~10 GHz.

The extra peaks in Fig. S5(a) possibly originate from the nearby GeV centers, whose associated D lines are shifted out of the measurement window thanks to the different impacts by the strain on transitions C and D [22,32,33].

To understand the photodynamics in the system, we study the power dependence of RF by varying either the resonant [Fig. 3(a)] or gating power [Fig. 3(e)]. By fitting each line with a Lorentzian function, we obtain a constant transition energy for different resonant powers [Fig. 3(b)], and observe a pronounced power broadening [Fig. 3(c)]. Meanwhile, the RF intensity displays an unconventional power dependence characterized by an unexpected drop at $\sim 3P_0$, as shown in Fig. 3(d), where $P_0 = 1.15 \pm 0.39$ μW is the resonant saturation power, determined by employing a pulse measurement scheme [22]. The drop of RF verifies the existence of a dark state, and indicates the opposite role played by the resonant laser to the gating beam, i.e., shelving the population into the dark state.

As the gating power increases, the initially irresolvable PLE spectrum starts to recover and then stabilizes at $\sim 10^{-5} P_1$ [Fig. 3(e)]. Through the evolution, the transition shows an exceptional stability by displaying zero drift of transition energy [Fig. 3(f)], and an unvarying excitation linewidth [Fig. 3(g)]. This superior optical property stems from the inversion symmetry of GeV center [29], and shows a striking contrast to the significant spectral diffusion displayed by NV centers under nonresonant excitation [34]. We attribute the broadening of linewidth for low gating powers ($<10^{-6} P_1$) to the detuning dependence of shelving efficiency of the entire system. Since the shelving becomes significantly stronger for smaller detuning (given a constant deshelving rate), it causes a flattening of PLE spectrum, and gives rise to a wider linewidth [22]. This is similar to the linewidth broadening observed in SiV center at millikelvin temperature, where spin pumping plays the role of shelving [35]. As the gating power increases, the gating-based dynamical rates are enhanced and finally dominate the population dynamics, thus stabilizing the linewidth to a constant value. When the gating power exceeds $10^{-3} P_1$, the RF intensity starts to drop, which is accompanied by a rising of PLE background produced by nonresonant excitation [Fig. 3(h)]. This reveals a competition between the resonant and nonresonant excitations.

The shelving effect induced by the resonant laser can be directly observed by modulating the resonant beam while keeping the nonresonant beam in cw mode, as shown in Fig. 4(a). The immediate exponential decay of RF following the excitation edge directly monitors the shelving process. The intensity of the transient peak reflects the population in the excited state before it is influenced by the shelving process induced by the resonant pumping. The subsequent plateau corresponds to the equilibrium state of the system dictated by both shelving and deshelving rates. Following this phenomenological picture, we construct a three-state model composed of a two-level system (G and E) and a dark state (D), as shown in Fig. 4(b). The population in the ground state (G) can be resonantly promoted (Ω) to the excited state (E), before relaxing back to the ground state via spontaneous decay ($\Gamma_{\rm sp}$), or being shelved into a dark state (D) via a nonradiative channel (k_{ED}). The ground and dark state can exchange the population at rates k_{DG} and k_{GD}, mainly enabled by nonresonant pumping. Within the framework of semiclassical picture, the time evolution of the system follows the master equation

$$\frac{d}{dt}(\rho_G,\ \rho_E,\ \rho_{GE},\ \rho_{EG},\ \rho_D)^T = \begin{pmatrix} -k_{GD} & \Gamma_{\rm sp} & i\Omega/2 & -i\Omega/2 & k_{DG} \\ 0 & -\Gamma_{\rm sp}-k_{ED} & -i\Omega/2 & i\Omega/2 & 0 \\ i\Omega/2 & -i\Omega/2 & -1/T_2 & 0 & 0 \\ -i\Omega/2 & i\Omega/2 & 0 & -1/T_2 & 0 \\ k_{GD} & k_{ED} & 0 & 0 & -k_{DG} \end{pmatrix} \begin{pmatrix} \rho_G \\ \rho_E \\ \rho_{GE} \\ \rho_{EG} \\ \rho_D \end{pmatrix}, \quad (1)$$

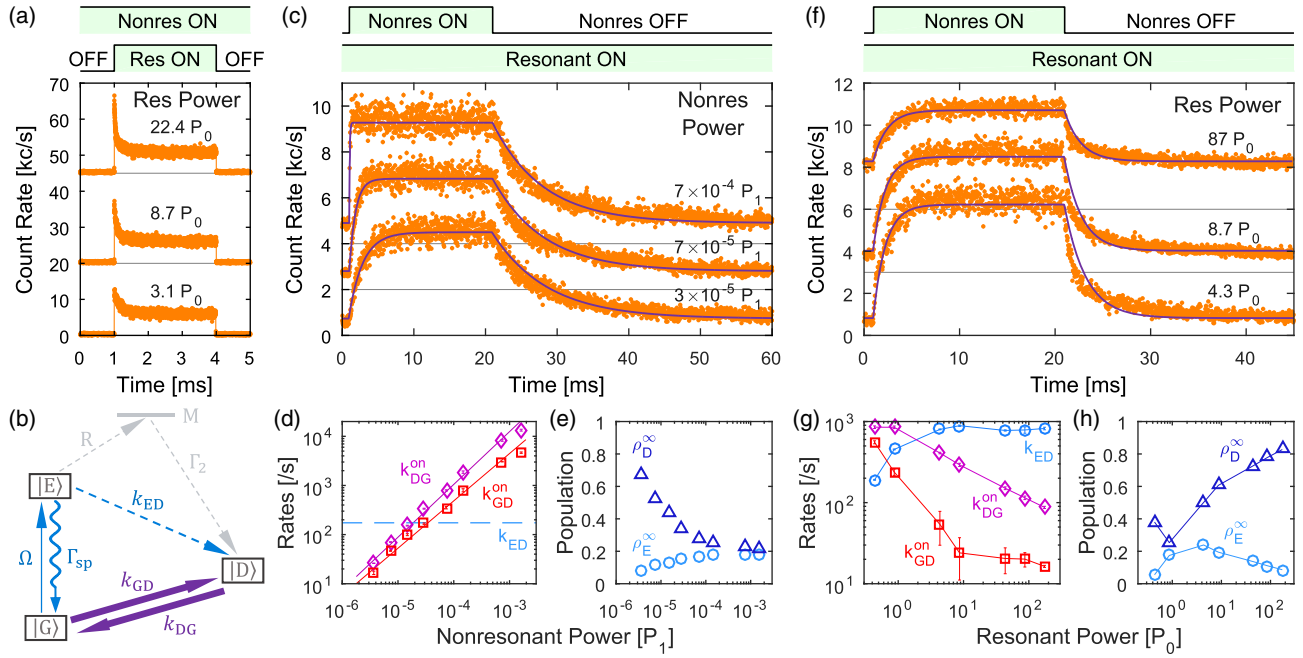

FIG. 4. Gating and shelving dynamics. (a) Time-resolved PL by modulating the resonant beam with constant nonresonant power of $7 \times 10^{-7} P_1$. (b) Physical model. G, E, D, and M: ground, excited, dark, and metastable state; k_{GD}, k_{DG}, and k_{ED}: population transfer rates from G to D, D to G, and E to D. Ω: resonant Rabi frequency; $\Gamma_{sp} = 1/T_1 = 280$ MHz: spontaneous decay rate, determined by lifetime measurement [22]. Gray arrows depict the possible physical processes underlying k_{ED}. (c) and (f) are the time-resolved PL by modulating the nonresonant beam with (c) constant resonant power ($0.9P_0$) or (f) constant nonresonant power ($7 \times 10^{-5} P_1$). Black curves are the fittings by using Eq. (3). (d) and (g) are the dynamical rates extracted from the fittings in (c) and (f), respectively. Dashed blue horizontal lines in (d) depict k_{ED}, representing its trivial nonresonant-power dependence in this experiment. Solid straight lines in (d) are the fittings with $k_{GD}^{on} = 3.5 \times 10^6 \times P^{0.96}$ (red) and $k_{DG}^{on} = 2.1 \times 10^7 \times P^{1.07}$ (purple), where P denotes the nonresonant power in the unit of P_1. (e) and (h) are the on-period steady-state population of dark state ρ_D^{∞} and two-level system ρ_E^{∞}, evaluated by using the rates in (d) and (g), respectively. In (a), (c), and (f), raw data (orange dots) are vertically shifted for clarity, with the zero-intensity level indicated by the gray horizontal lines. Top panel: modulation protocol.

where ρ_G, ρ_E, and ρ_D are the time-dependent population in ground, excited, and dark state, ρ_{GE} and ρ_{EG} are the coherence between G and E, Ω is the resonant Rabi frequency, Γ_{sp} is the spontaneous decay rate, and T_2 is the coherence time of excited state. Note that Eq. (1) has incorporated the effect of stimulated emission, which is expected to play a nontrivial role in population dynamics of the system. The excitation linewidth can be derived from the steady-state solution of Eq. (1)

$$\Delta\nu = \frac{1}{\pi T_2}\sqrt{1 + \frac{1}{2}\frac{\Omega^2 T_2}{\Gamma_{sp} + k_{ED}}\left(1 + \frac{k_{ED} + k_{DG}}{k_{DG} + k_{GD}}\right)} \quad (2)$$

in the unit of linear frequency. By equalizing the asymptotic linewidth at $0P_0$ in Fig. 3(c) ($\sim$1 GHz, 20 times the lifetime-limited value) to Eq. (2) with $\Omega = 0$, we obtain $T_2 = 316 \pm 20$ ps, which is consistent with the coherence time extracted from the Rabi oscillations measurement [Fig. 2(d)]. The detected RF intensity follows

$$I_{PL}(t) = \eta \Gamma_{sp} \rho_E(t), \quad (3)$$

where $\eta = 9 \times 10^{-5}$ is the overall efficiency including both detection efficiency of the experimental setup and quantum yield of GeV center [22,36].

To extract the dynamical rates of gating and shelving, we perform a similar time-resolved experiment, but modulating the nonresonant beam while keeping the resonant beam in cw mode. Here, the PL inherits the modulation pattern of the gating laser, and displays a gating-power-dependent modulation depth, as shown in Fig. 4(c). Since the nonresonant laser has little effect on k_{ED}, we keep this rate a constant and determine it via global fitting [22]. The main effect of the gating beam is to promote k_{GD} and k_{DG} linearly over the nonresonant power, as show in Fig. 4(d). This power dependence implies a single-photon process for the shelving and deshelving of population induced by the nonresonant laser. Consequentially, the steady-state population is transferred from the dark state to the ground and excited states as increasing the gating power, as shown in Fig. 4(e).

Resonant-power dependence is shown in Fig. 4(f). The main effect of the resonant laser is to speed up the shelving rate k_{ED}, while indirectly reducing rates k_{GD} and k_{DG}, as shown in Fig. 4(g). The saturation behavior of k_{ED} implies a two-step shelving process mediated by a metastable state

M, as shown by the gray arrows in Fig. 4(b). The first step of population pumping (R) from the excited state to the metastable state is responsible for the enhancement of k_{ED}, while the second step of nonradiative decay (Γ_2) from the metastable state to the dark state caps k_{ED} at kHz regime. The peak of steady-state population ρ_E^∞ at several P_0 in Fig. 4(h) suggests the optimal resonant power for the maximum RF given a gating power.

Now we briefly discuss the photophysics of the GeV system by comparing it to NV centers in diamond [17,37] and InGaAs self-assembled quantum dots (QD) [38,39], where a similar phenomenon has been observed. For both systems, the dark state has been identified as a differently charged species of the emitter, specifically, positively charged QD [30] and neutrally charged NV center [40]. It is hence plausible that the dark state of the GeV center is also a differently charged state (i.e., neutral) [27]. For all three systems, the gating of RF can be achieved by employing a small amount of nonresonant beam. The mechanism for NV centers and QDs involves a local free-charge-carrier bath produced by the light, which can modify the charge dynamics of the emitter in favor of resonant excitation. We argue a similar mechanism for GeV center as long as nonresonant laser is employed, which is substantiated by two observations: linear power dependence of k_{DG} and k_{GD} [Fig. 4(d)], and identical gating efficiency for 405 and 532 nm nonresonant beams [Fig. 2(a)].

On the other hand, the shelving mechanism induced by resonant pumping is different. For QDs, no such shelving channel is reported. For NV centers, a two-photon process is involved based on the quadratic power dependence of the dynamical rates [17,18]. For the GeV center, a two-step shelving mechanism pivot by a metastable state and nonradiative decay channel is identified in this Letter. Finally, the decrease of rates k_{GD} and k_{DG} in Fig. 4(g) is possibly related to the decrease of free charge carrier density, caused by the presence of more charge traps in the area as induced by a stronger resonant beam [22].

In summary, we demonstrated the shelving effect induced by the resonant laser in GeV centers, which can be counteracted by introducing a weak nonresonant repumping laser. The dynamics of shelving and gating can be quantitatively explained by the presence of a dark state, while the identity of this dark state warrants future investigation. We stress that this gating phenomenon is quite general and ubiquitous, not limited to the specific center investigated in this Letter [22]. The recovery and stabilization of the RF could be useful for quantum information science and scalable quantum photonics, such as spin-photon entanglement [41,42] and photon interferences [11].

We acknowledge support from the Singapore NRF fellowship grant (No. NRF-NRFF2015-03) and NRF QEP grant, Singapore Ministry of Education [MOE2016-T2-2-077, MOE2016-T2-1-163, and MOE2016-T3-1-006 (S)], A*Star QTE programme, the Australian Research council (via DP180100077), the Asian Office of Aerospace Research and Development Grant No. FA2386-17-1-4064, the Office of Naval Research Global (N62909-18-1-2025), and the AFAiiR node of the NCRIS Heavy Ion Capability for access to ion-implantation and ion-beam analysis facilities.

*These two authors contributed equally to this work.
†igor.aharonovich@uts.edu.au
‡wbgao@ntu.edu.sg

[1] I. Aharonovich and E. Neu, Adv. Opt. Mater. **2**, 911 (2014).
[2] M. Atatüre, D. Englund, N. Vamivakas, S.-Y. Lee, and J. Wrachtrup, Nat. Rev. Mater. **3**, 38 (2018).
[3] E. Neu, D. Steinmetz, J. Riedrich-Mller, S. Gsell, M. Fischer, M. Schreck, and C. Becher, New J. Phys. **13**, 025012 (2011).
[4] T. Iwasaki, F. Ishibashi, Y. Miyamoto, Y. Doi, S. Kobayashi, T. Miyazaki, K. Tahara, K. D. Jahnke, L. J. Rogers, B. Naydenov, F. Jelezko, S. Yamasaki, S. Nagamachi, T. Inubushi, N. Mizuochi, and M. Hatano, Sci. Rep. **5**, 12882 (2015).
[5] Y. N. Palyanov, I. N. Kupriyanov, Y. M. Borzdov, and N. V. Surovtsev, Sci. Rep. **5**, 14789 (2015).
[6] S. Häuβler, G. Thiering, A. Dietrich, N. Waasem, T. Teraji, J. Isoya, Takayuki Iwasaki, M. Hatano, F. Jelezko, A. Gali, and A. Kubanek, New J. Phys. **19**, 063036 (2017).
[7] M. K. Bhaskar, D. D. Sukachev, A. Sipahigil, R. E. Evans, M. J. Burek, C. T. Nguyen, L. J. Rogers, P. Siyushev, M. H. Metsch, H. Park, F. Jelezko, M. Lončar, and M. D. Lukin, Phys. Rev. Lett. **118**, 223603 (2017).
[8] H. Siampour, S. Kumar, V. A. Davydov, L. F. Kulikova, V. N. Agafonov, and S. I. Bozhevolnyi, Light Sci. Appl. **7**, 61 (2018).
[9] K. Bray, B. Regan, A. Trycz, R. Previdi, G. Seniutinas, K. Ganesan, M. Kianinia, S. Kim, and I. Aharonovich, ACS Photonics **5**, 4817 (2018).
[10] C. Hepp, T. Müller, V. Waselowski, J. N. Becker, B. Pingault, H. Sternschulte, D. Steinmüller-Nethl, A. Gali, J. R. Maze, M. Atature, and C. Becher, Phys. Rev. Lett. **112**, 036405 (2014).
[11] A. Sipahigil, K. D. Jahnke, L. J. Rogers, T. Teraji, J. Isoya, A. S. Zibrov, F. Jelezko, and M. D. Lukin, Phys. Rev. Lett. **113**, 113602 (2014).
[12] E. Neu, M. Fischer, S. Gsell, M. Schreck, and C. Becher, Phys. Rev. B **84**, 205211 (2011).
[13] L.-M. Duan, M. D. Lukin, J. I. Cirac, and P. Zoller, Nature (London) **414**, 413 (2001).
[14] D. Bouwmeester, J.-W. Pan, K. Mattle, M. Eibl, H. Weinfurter, and A. Zeilinger, Nature (London) **390**, 575 (1997).
[15] J.-W. Pan, D. Bouwmeester, H. Weinfurter, and A. Zeilinger, Phys. Rev. Lett. **80**, 3891 (1998).
[16] M. W. Doherty, N. B. Manson, P. Delaney, F. Jelezko, J. Wrachtrup, and L. C. L. Hollenberg, Phys. Rep. **528**, 1 (2013).
[17] G. Waldherr, J. Beck, M. Steiner, P. Neumann, A. Gali, T. Frauenheim, F. Jelezko, and J. Wrachtrup, Phys. Rev. Lett. **106**, 157601 (2011).

[18] P. Siyushev, H. Pinto, M. Voros, A. Gali, F. Jelezko, and J. Wrachtrup, Phys. Rev. Lett. **110**, 167402 (2013).
[19] D. D. Sukachev, A. Sipahigil, C. T. Nguyen, M. K. Bhaskar, R. E. Evans, F. Jelezko, and M. D. Lukin, Phys. Rev. Lett. **119**, 223602 (2017).
[20] A. N. Vamivakas, C.-Y. Lu, C. Matthiesen, Y. Zhao, S. Fält, A. Badolato, and M. Atatre, Nature (London) **467**, 297 (2010).
[21] H. J. Kimble, Nature (London) **453**, 1023 (2008).
[22] See Supplemental Material at http://link.aps.org/supplemental/10.1103/PhysRevLett.123.033602 for sample preparation, resonant saturation power measurement, modeling of dark-state dynamics, and experiments on other GeV centers, which includes Refs. [23–26].
[23] R. Loudon, *The Quantum Theory of Light*, 3rd ed. (Oxford University Press, New York, 2000).
[24] Y.-I. Sohn, S. Meesala, B. Pingault, H. A. Atikian, J. Holzgrafe, M. Gündoğan, C. Stavrakas, M. J. Stanley, A. Sipahigil, J. Choi, M. Zhang, J. L. Pacheco, J. Abraham, E. Bielejec, M. D. Lukin, M. Atatüre, and M. Lončar, Nat. Commun. **9**, 2012 (2018).
[25] A. V. Turukhin, C.-H. Liu, A. A. Gorokhovsky, R. R. Alfano, and W. Phillips, Phys. Rev. B **54**, 16448 (1996).
[26] E. Neu, M. Agio, and C. Becher, Opt. Express **20**, 19956 (2012).
[27] G. Thiering and A. Gali, Phys. Rev. X **8**, 021063 (2018).
[28] L. Marseglia, J. P. Hadden, A. C. Stanley-Clarke, J. P. Harrison, B. Patton, Y.-L. D. Ho, B. Naydenov, F. Jelezko, J. Meijer, P. R. Dolan, J. M. Smith, J. G. Rarity, and J. L. O'Brien, Appl. Phys. Lett. **98**, 133107 (2011).
[29] P. Siyushev, M. H. Metsch, A. Ijaz, J. M. Binder, M. K. Bhaskar, D. D. Sukachev, A. Sipahigil, R. E. Evans, C. T. Nguyen, M. D. Lukin, P. R. Hemmer, Y. N. Palyanov, I. N. Kupriyanov, Y. M. Borzdov, L. J. Rogers, and F. Jelezko, Phys. Rev. B **96**, 081201(R) (2017).
[30] H. S. Nguyen, G. Sallen, M. Abbarchi, R. Ferreira, C. Voisin, P. Roussignol, G. Cassabois, and C. Diederichs, Phys. Rev. B **87**, 115305 (2013).
[31] A. Delteil, W.-B. Gao, P. Fallahi, J. Miguel-Sanchez, and A. Imamoglu, Phys. Rev. Lett. **112**, 116802 (2014).
[32] S. Maity, L. Shao, Y.-I. Sohn, S. Meesala, B. Machielse, E. Bielejec, M. Markham, and M. Loncar, Phys. Rev. Applied **10**, 024050 (2018).
[33] S. Meesala, Y.-I. Sohn, B. Pingault, L. Shao, H. A. Atikian, J. Holzgrafe, M. Gündoğan, C. Stavrakas, A. Sipahigil, C. Chia, R. Evans, M. J. Burek, M. Zhang, L. Wu, J. L. Pacheco, J. Abraham, E. Bielejec, M. D. Lukin, M. Atature, and M. Lončar, Phys. Rev. B **97**, 205444 (2018).
[34] J. Wolters, N. Sadzak, A. W. Schell, T. Schroder, and O. Benson, Phys. Rev. Lett. **110**, 027401 (2013).
[35] J. N. Becker, B. Pingault, D. Gross, M. Gundogan, N. Kukharchyk, M. Markham, A. Edmonds, M. Atature, P. Bushev, and C. Becher, Phys. Rev. Lett. **120**, 053603 (2018).
[36] Special Issue in honor of Professor Renata Reisfeld for her outstanding contributions to luminescent inorganic glasses, edited by K. N. Boldyrev, B. N. Mavrin, P. S. Sherin, and M. N. Popova [J. Lumin. **193**, 119 (2018)].
[37] K.-M. C. Fu, C. Santori, P. E. Barclay, and R. G. Beausoleil, Appl. Phys. Lett. **96**, 121907 (2010).
[38] H. S. Nguyen, G. Sallen, C. Voisin, P. Roussignol, C. Diederichs, and G. Cassabois, Phys. Rev. Lett. **108**, 057401 (2012).
[39] D. Chen, G. R. Lander, K. S. Krowpman, G. S. Solomon, and E. B. Flagg, Phys. Rev. B **93**, 115307 (2016).
[40] N. Aslam, G. Waldherr, P. Neumann, F. Jelezko, and J. Wrachtrup, New J. Phys. **15**, 013064 (2013).
[41] E. Togan, Y. Chu, A. S. Trifonov, L. Jiang, J. Maze, L. Childress, M. V. G. Dutt, A. S. Sørensen, P. R. Hemmer, A. S. Zibrov, and M. D. Lukin, Nature (London) **466**, 730 (2010).
[42] K. De Greve, L. Yu, P. L. McMahon, J. S. Pelc, C. M. Natarajan, N. Y. Kim, E. Abe, S. Maier, C. Schneider, M. Kamp, S. Höfling, R. H. Hadfield, A. Forchel, M. M. Fejer, and Y. Yamamoto, Nature (London) **491**, 421 (2012).